High-Reynolds Number Circulation Control Testing in the National Transonic Facility (Invited)

William E. Milholen, II[1], Gregory S. Jones[2], David T. Chan[3],
and Scott L. Goodliff[4]
NASA Langley Research Center, Hampton, VA, 23681

A new capability to test active flow control concepts and propulsion simulations at high Reynolds numbers in the National Transonic Facility at the NASA Langley Research Center is being developed. The first active flow control experiment was completed using the new FAST-MAC semi-span model to study Reynolds number scaling effects for several circulation control concepts. Testing was conducted over a wide range of Mach numbers, up to chord Reynolds numbers of 30 million. The model was equipped with four onboard flow control valves allowing independent control of the circulation control plenums, which were directed over a 15% chord simple-hinged flap. Preliminary analysis of the uncorrected lift data showed that the circulation control increased the low-speed maximum lift coefficient by 33%. At transonic speeds, the circulation control was capable of positively altering the shockwave pattern on the upper wing surface and reducing flow separation. Furthermore, application of the technique to only the outboard portion of the wing demonstrated the feasibility of a pneumatic based roll control capability.

Nomenclature

b = wing span
c = local wing chord
C_D = drag coefficient
C_L = lift coefficient
C_m = pitching moment coefficient
C_p = surface pressure coefficient
C_μ = momentum coefficient, Equation 1
h = blowing slot height
M = local value of Mach number
M_∞ = freestream Mach number
$\dot{m}$ = mass flow
NPR = nozzle pressure ratio, $(p_o)_{jet}/p_\infty$
NPR_{exit} = nozzle exit pressure ratio, $(p_o)_{jet}/p_{exit}$
p = pressure
q_∞ = freestream dynamic pressure
Re = Reynolds number based on mean aerodynamic chord
S = wing reference area
s = local arc length

T = temperature
U_{jet} = total velocity at jet exit
x,y,z = Cartesian coordinate system

α = angle of attack
η = non-dimensional semi-span location
ρ = density

subscripts
jet = jet exit location
o = stagnation quantity
∞ = freestream quantity

---

[1] Research Engineer, Configuration Aerodynamics Branch, Mail Stop 499, AIAA Senior Member
[2] Research Engineer, Flow Physics and Control Branch, Mail Stop 170, AIAA Senior Member
[3] Research Engineer, Configuration Aerodynamics Branch, Mail Stop 499, AIAA Member
[4] Test Engineer, Jacobs Technology, Inc., Mail Stop 267, AIAA Senior Member

I. Introduction

Many of the advanced aircraft being designed today utilize active flow control systems that closely integrate with both the engine and airframe[1,2,3]. Cruise efficiency, community noise, and runway independence can no longer be optimized independently because of the close coupling of the engine, airframe, and wing. Evaluating the benefits of active flow control systems on scaled wind tunnel models requires added attention to detail. Not only does the outer mold line of the model need to accurately represent the proposed flight vehicle, but also the intricate details of the flow control system[4]. If the flow control system adds or removes a net mass to the flow field, it is necessary to accurately characterize the mass flow and document the fluid conditions at the relevant model interface locations. It is desirable that the wind tunnel testing should be conducted at Reynolds

Figure 1: Aerial view of the NTF.

numbers that are representative of flight conditions, to document the appropriate scaling parameters, and ensure the active flow control technique is properly scaled to the flight vehicle. This paper focuses on the first active flow control experiment conducted in the National Transonic Facility (NTF) at the NASA Langley Research Center, Figure 1.   The new Fundamental Aerodynamics Subsonic/Transonic-Modular Active Control (FAST-MAC) model was used to test circulation control concepts at realistic flight Reynolds numbers at both low-speed and transonic cruise conditions.

Circulation control techniques have experienced a resurgence recently, with many research efforts focusing on developing databases for CFD validation[5,6,7,8,9,10], as unreliable predictions have been a barrier to applying the techniques to aircraft.   As with most publically available active flow control datasets, one shortfall remains the lack of Reynolds number scaling data, which could limit the application of the technique to flight conditions.   The FAST-MAC model, depicted in Figure 2 in the high-lift mode, was developed to allow active flow control techniques such as circulation control to be tested at realistic flight Reynolds numbers in the NTF.   The model is modular, allowing nearly all wing components to be replaced, and is well suited for future testing of other flow control concepts. Even though the wing has a moderate aspect ratio, the wing design is considered to represent the state-of-the-art in transonic wing design[11,12] and is an open geometry that can be distributed to the research community. The model is also unique in that it will allow
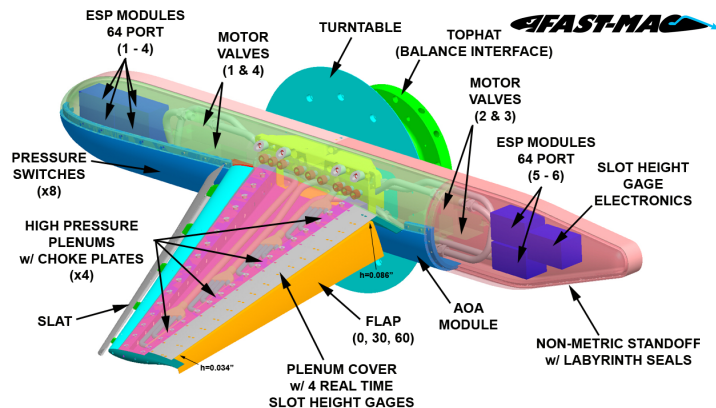

Figure 2: Cutaway view of the FAST-MAC model, in high-lift mode, highlighting multiple internal flow paths.

circulation control strategies to be evaluated at transonic Mach numbers, where little research has been published[13].

In the low-speed high-lift mode, the circulation control is applied as shown in Figure 3, where a high momentum jet from a blowing slot is directed over a simple short-chord hinged flap[14]. The jet flow from the blowing slot is typically characterized by the non-dimensional blowing coefficient C_μ[15], defined by equation 1. The non-dimensional slot height, h/c, and the plenum stagnation pressure are the key parameters defining the maximum jet velocity[16], U_{JET}. The model was designed to allow the circulation control to be manipulated by four independent plenums across the span of the wing, each with a computer-controlled valve located in the fuselage. A unique suite of instrumentation was developed to document the internal and external flow features of the model.
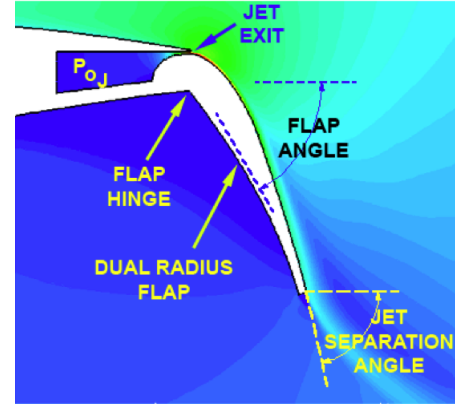

Figure 3: Circulation control blowing slot nomenclature.

$$C_\mu = \frac{Thrust}{q_\infty S} = \frac{2hb_{jet}}{cb} \frac{\rho_{jet}}{\rho_\infty} \frac{U^2_{jet}}{U^2_\infty} = \frac{\dot{m}U_{jet}}{q_\infty S} \qquad (1)$$

The model was tested over a wide variation of Mach and Reynolds numbers to investigate the effect of various circulation control techniques. In addition to being the first active flow control test in the NTF, the test was also the first transonic semi-span test conducted in the facility, and the first to use the new higher capacity NTF-117S semi-span force and moment balance. The discussion to follow will give an overview of the testing methodology, and provide a preliminary assessment of the key data results that were observed.

II. Experimental Setup

A. Wind Tunnel Description

The NTF is one of a limited number of wind tunnel facilities that can achieve flight Reynolds numbers and Mach numbers for transport type aircraft for both cruise and high lift operations. The tunnel is a fan-driven, closed-circuit, continuous-flow, pressurized wind tunnel capable of operating either in dry air at warm temperatures or in nitrogen gas from warm to cryogenic temperatures,
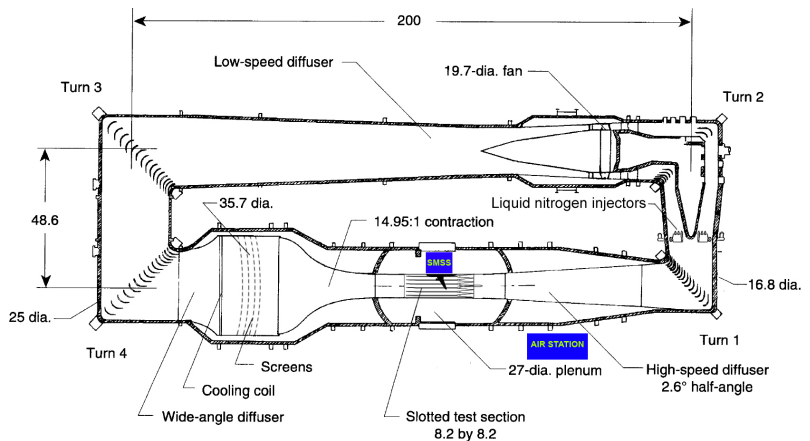

Figure 4: Layout of the NTF circuit, including the high-pressure air delivery station, and the SMSS, dimensions in feet.

3
American Institute of Aeronautics and Astronautics

Figure 4. The test section is 8.2 ft by 8.2 ft in cross section, and 25 ft in length. The test section floor and ceiling are slotted, and the sidewalls are solid. Semi-span models are mounted in the tunnel using the Sidewall Mounted Support System (SMSS). The wind tunnel is capable of an absolute pressure range from 1 atmosphere to 8.8 atmospheres, a practical temperature range from -270°F to 130°F, a Mach number range from 0.1 to 1.2, and a maximum Reynolds number of 146x10^6 per foot at Mach 1. Typical tests use a temperature range from -250$^°$F to 120$^°$F. For tests that utilize the high-pressure air delivery station to enable flow control or propulsion simulation systems, the lower temperature limit is set to -50$^°$F to simplify the testing technique.

The dual flow high-pressure air station[17] is coupled to the SMSS as shown in Figure 5. The two independently controlled air lines pass through the center of the force and moment balance, and couple to the model using a concentric bellows arrangement. The model is protected from over pressurization by the model protection system. The maximum pressure limit can be adjusted independently for both legs from 300 psi to 1200 psi. If the set pressure matches or exceeds the safety limit for the wind tunnel model, then the supply line into the SMSS would be isolated and vented in less than 0.5 seconds.
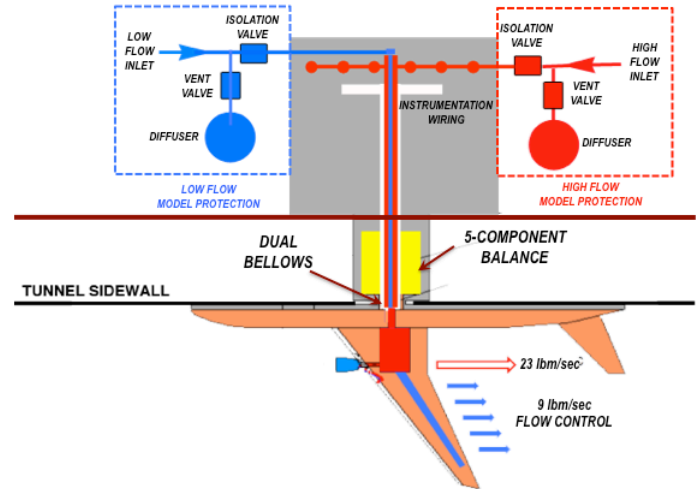

Figure 5: Diagram of high-pressure air routing to a semi-span model mounted on the sidewall of the NTF.

B. Model Description

The FAST-MAC model shown in Figure 6 has a modern supercritical wing and was designed to become an NTF standard for evaluating performance characteristics of integrated active flow control and propulsion systems. The outer mold line of the model was designed for a cruise Mach number of 0.85, a lift coefficient of 0.50, at a Reynolds number based on mean aerodynamic chord of 30x10^6. The wing was designed with the unstructured Navier-Stokes flow solver USM3D in conjunction with the CDISC design code[11]. A

Figure 6: Planform view of the FAST-MAC semi-span model.

tangential blowing slot is located at the 85% chord location on the upper surface, and is directed over a 15% chord simple hinged flap for both the cruise and high-lift configurations. For transonic testing, the non-dimensional blowing slot height was set to h/c = 0.0019. The wing has an aspect ratio of 5.0, taper ratio of 0.40, a leading edge sweep of 30$^°$, zero dihedral, and a reference area of 6.06 ft^2. The CDISC design method produced a linear twist distribution with 5.0$^°$ of washout. The chord length at the side of the fuselage is 25.0 inches, resulting in a mean
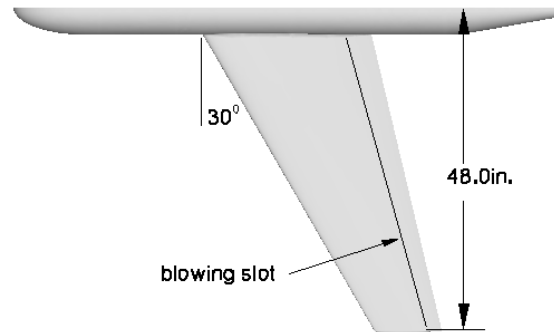
aerodynamic chord of 19.4 inches. The generic fuselage is comprised of circular cross sections with a maximum width of 5.0 inches, and a length of 82.0 inches. The wing is mounted in the mid-fuselage position to simplify the routing of the high-pressure air supply lines. The model is offset from the tunnel sidewall using a 2.0-inch non-metric standoff[18], which has a profile shape identical to that of the fuselage centerline. A labyrinth type flow blocker is used to minimize the flow between the non-metric standoff and the fuselage, while a set of contact sensors are used to indicate mechanical fouling during the testing. The back of the stand-off is equipped with a spring loaded Teflon flow blocker that scrubs

Figure 7: FAST-MAC model in cruise configuration mounted on the sidewall in the NTF.

against the tunnel sidewall, filling the nominal gap of 0.125 inches between the stand-off and the tunnel wall. Figure 7 shows a photograph of the model installed in the test section.
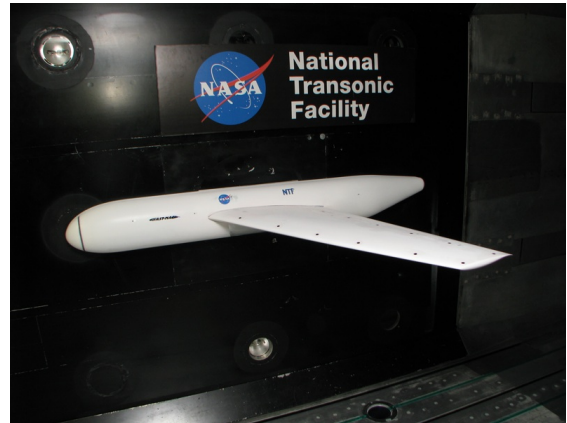
Figure 8 shows a CAD rendering of the model configured for low-speed high-lift testing, with a $60°$ deflection of the hinged trailing-edge flap, and a non-dimensional blowing slot height of h/c=0.0031. The main wing leading edge is protected from premature flow separation by a leading edge slat with an average deflection angle of $25°$ with respect to the *cruise* leading edge. It should be noted that although the cruise leading edge is a removable model piece, the slat does *not* simulate the deployment of the cruise leading edge, which would occur on an actual aircraft. This does have a slight impact on the maximum

Figure 8: FAST-MAC model configured for high-lift testing with $60°$ flap.

obtainable lift coefficient, but was deemed an acceptable compromise for the present research. An intermediate $30°$ trailing edge flap was fabricated, but not tested.

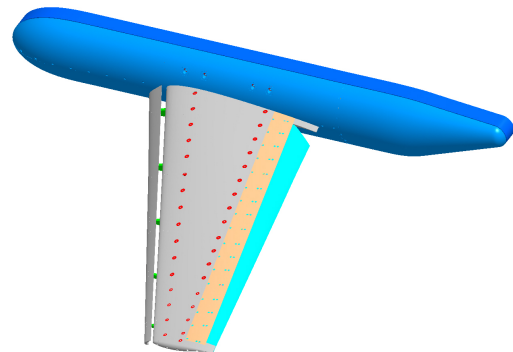The wing was instrumented with four chordwise rows of static pressure taps at semi-span locations of: $\eta = 0.20, 0.40, 0.60,$ and 0.80. The fuselage had a row of taps along the centerline plane ($\eta = 0.00$), as well as a radial row ahead of the wing, giving a total of 249 pressure taps on the model. The surface pressures were measured using Electronically Scanned Pressure (ESP) modules mounted inside the forward fuselage. The selection of ESP modules was driven by both the expected sonic conditions at the exit of the blowing slot, as well as the transonic portion of the test. The module sizes used ranged from 5 psid to 100 psid. Post-test uncertainty analysis of the pressure data yielded the following 1-σ repeatability values, for each Mach number range. For the low-speed high-lift testing the repeatability of the C_p measurements on the wing were ±0.04, while on the flap it increased to ±0.47. For the transonic phase of testing the repeatability value on the wing was ±0.009, while the flap it was ±0.019. The larger values on the flap are in part due to the 100 psid module.

The FAST-MAC model utilized four flow paths to achieve independent lift and thrust performance along the span of the circulation control flap, as shown previously in Figure 2. Each plenum section was fed by a flow control valve located in the fuselage via a rapid diffuser located in the wing box, where the outboard plenum is shown in Figure 9. The diffuser is used to subdivide the incoming flow to the plenum, allowing it to be supplied at four evenly spaced spanwise locations. A 33.4% open area choke plate is installed on the downstream side of the rear wing box spar, and was intended to measure the mass flow and improve flow uniformity. The flow then enters the aft plenum region of the model, where the upper plenum cover is supported by the streamlined standoffs, which are used to set the blowing slot height. A nominal cross sectional view between the standoffs is shown in Figure 10 for the 60° flap deflection. At the slot exit, $h/c = 0.0031$, this corresponds to a 6 to 1 contraction ratio. For the transonic cruise
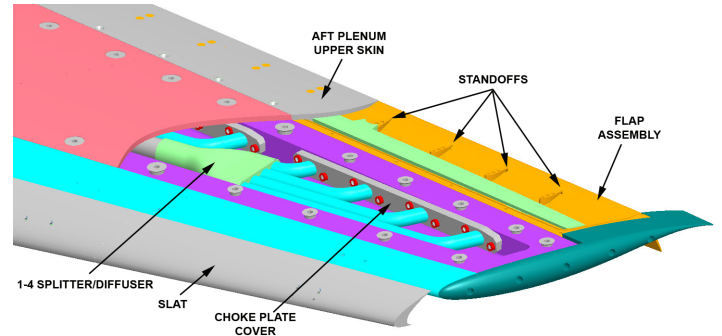

Figure 10: Cutaway sketch of the outboard plenum highlighting the flow path.
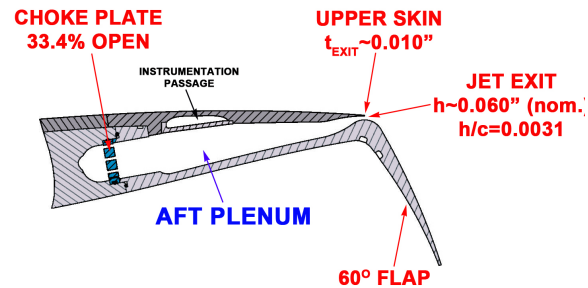
Figure 9: Cross sectional sketch of aft plenum region on FAST-MAC model.

configuration a zero degree flap deflection is used with $h/c = 0.0019$, giving a slot exit contraction ratio of 12 to 1. The slot height for both configurations was set using laser cut shims, to maintain a slot height accuracy of 0.0005 in. along the span. The slot height was measured real time with capacitance type gages[19] throughout the tests at four spanwise locations to capture slot height movement due to internal pressure or temperature variations. Although the data will not be presented, the slot height varied less than 1% at the maximum plenum pressure, and was not a function of temperature.

Each of the four aft plenums was instrumented with redundant total pressure and total temperature measurements, as well as static pressure measurements upstream and downstream of the choke plates. In addition, the external static pressure tap distribution on the *upper* flap surfaces was continued into the plenum region, to characterize the acceleration of the flow as it exited the blowing slot.

C. NTF-117S Balance and Pressure Tare Corrections

As noted earlier, this was the first transonic semi-span test conducted in the NTF and required the new NTF-117S balance[20] to measure the forces and moments on the model. The use of the bellows, shown in Figure 11, to connect the model to the high-pressure air delivery system requires that an additional pressure tare correction be applied to the
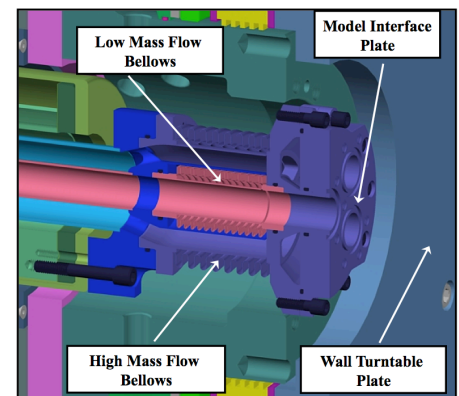

Figure 11: Cross sectional view of the bellows at the model attachment location.

American Institute of Aeronautics and Astronautics

balance measurements to account for the added and variable stiffness that the pressurized bellows creates. The pressure tare calibration could not be performed in a calibration laboratory due to the complexity of the piping arrangement inside the SMSS. A new capability has been developed to perform a full pressure tare calibration at the NTF, with the balance mounted inside the SMSS. During this calibration the loading fixture began to flex beyond acceptable tolerances, and only approximately half of the pressure tare calibration could be completed before the wind tunnel testing began. Since the completion of the wind tunnel testing, the deficiencies in the calibration hardware have been addressed, and the pressure tare calibration was recently completed. Thus, only limited *uncorrected* force and moment data will be presented below.

D.   High-Pressure Air Delivery System

The air delivery system is a permanent high-pressure air system that provides a continuous source of clean, dry air. The system was designed to provide a total weight flow of 32 lbm/sec divided into two flow paths. The dual flow system consists of two independent air supply lines that are tied to the SMSS used for semi-span testing. The FAST-MAC model utilized only a single leg of this system as shown in the schematic in Figure 12. This leg is equipped with a coarse and fine control valve and has a Multiple Critical Venturi (MVC) system[21] and a redundant vortex flow metering system located outside the tunnel plenum to capture the total mass flow. The MCV can measure the mass flow to within 0.1 percent of actual reading[17]. The total temperature of the model air stream can be set from $0°F$ to $120°F$ by using a steam heating system. The low temperature settings are dependent on Joule Thompson effects and thermal conduction associated with the piping located in the low temperature environment of the wind tunnel plenum.
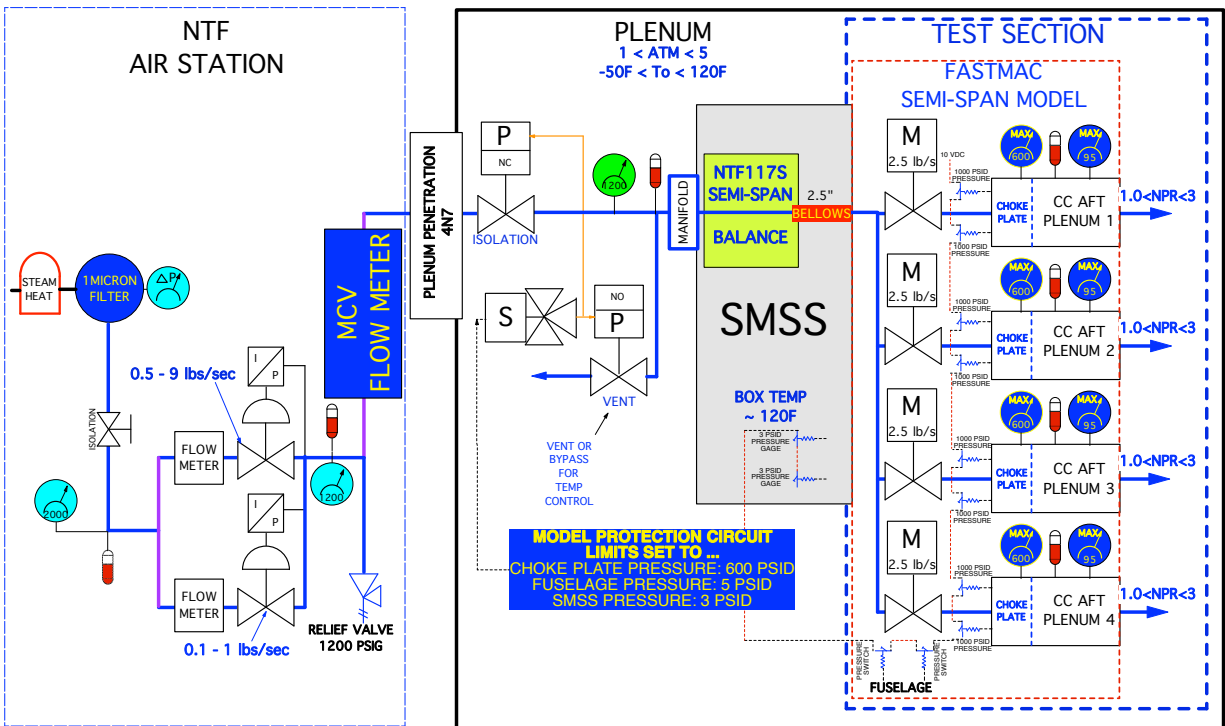

Figure 12:   Schematic of the high-pressure air delivery system for the FAST-MAC model.

American Institute of Aeronautics and Astronautics

An example of the correlation of mass flow and NPR is shown in Figure 13 for selected free stream Mach numbers utilizing an averaged slot height of 0.060 inches for the high lift configuration and 0.0375 inches for the cruise configuration. This example represents the maximum mass flow requirements for the FAST-MAC model and illustrates the large range of momentum coefficients required for this test.
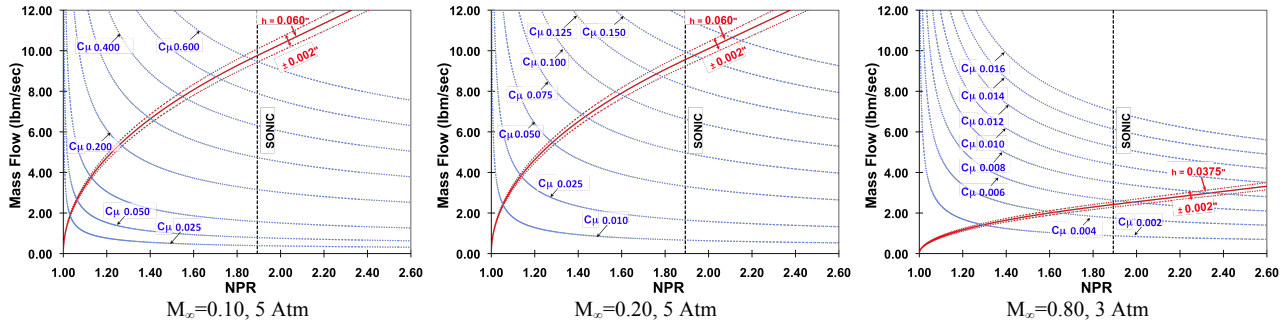

M_∞=0.10, 5 Atm M_∞=0.20, 5 Atm M_∞=0.80, 3 Atm

Figure 13: **Mass flow requirements for the FAST-MAC model, T_o=-50°F, $(T_o)_{jet}$=0°F.**

E. Test Conditions

The low-speed high-lift portion of the testing was primarily conducted at a freestream Mach number of 0.20, while a limited dataset was obtained at Mach 0.10. The test Reynolds number range was 5.0, 10.0 and 15.0 million. The angle-of-attack was varied from -20$^°$ to 27$^°$. The transonic portion of the test focused on Mach numbers from 0.70 to 0.88. The Reynolds numbers based on the mean chord were 10.0, 15.0, 20.0 and 30 million. An aeroelastic step was included at the 15.0 million Reynolds number to assess any model flexibility effects. For Mach numbers below 0.84, the angle-of-attack range was -12$^°$ to 12$^°$, for the remaining Mach numbers, the range was -6$^°$ to 6$^°$. The tunnel stagnation temperature range for both portions of the experiment was -50$^°$F to 120$^°$F. Data was also obtained to characterize the model deformations using the Video Model Deformation system, however this data will not be presented.

III. Results

Before the experimental results are discussed, several operational characteristics of the testing will be highlighted. Initial component level cryogenic cycling revealed that the onboard control valves lacked sufficient torque to actuate when pressurized to 1000 psi, which required modification of the gearing package. The FAST-MAC model was assembled and cryogenically cycled before installation in the test section. A thorough leak check procedure was developed to ensure the model plumbing performed as designed. An acceptable leak rate for the model when pressurized to 1000 psi was 20 psi/hr. Once installed in the test section, a similar leak check procedure was used to verify a nearly identical leak rate, including the supply piping inside the SMSS. The leak rate of the system was verified several times during the experiment, and at the conclusion of testing.

American Institute of Aeronautics and Astronautics

During tunnel testing, care was taken to condition the air station and model flow path to obtain stable flow path temperatures during data runs. This was accomplished with little impact to testing productivity while the tunnel circuit was being conditioned. The facility heating system was bypassed, providing a consistent inlet temperature to the high-pressure air station during the testing. The aft plenum temperatures in the model were monitored and found to be a good indicator of the temperature stability prior to testing. Once this was achieved, all tunnel systems were brought down for wind-off zero calibrations, and calibration of the ESP systems. As the tunnel was brought back to testing conditions, the model flow path was observed to return quickly to steady state temperatures, and thus ready for taking data.

The FAST-MAC model performed well through all phases of the testing, but suffered from one unexpected setback. The four choke plates installed in the aft plenum region did not choke, due to unexpected losses in the internal flow path. As a result, the choke plates only performed as flow straightening devices. The stagnation pressure measurements in the four plenums were uniform, and testing proceeded. Although the total mass flow through the model was accurately measured by the air station MCV, the lack of local flow metering via the plenum choke plates makes it more difficult to document the spanwise variation of the mass flow, and complicates the removal of the added thrust from the measured forces and moments. Lastly, only limited *uncorrected* force and moment data will be presented below as appropriate, since the new pressure tare correction for the NTF-117S balance has just become available. The surface pressure data on the wing will be used to highlight the observations that follow, and are adequate to illustrate the observed flow physics.

A. Data Repeatability Analysis

The testing matrix was planned to incorporate several sets of repeat runs for the various conditions that were tested. Typcially the repeat runs were separated by data runs at alternate flow conditions, including different Mach numbers in the transonic portion of the test. Some of the repeat sets featured back-to-back repeat polars. Given the number of "firsts" for this test as discussed in the introduction, including the new NTF-117S balance and bellows arrangement, more analysis is required to make definitive claims regarding the repeatability for the test. Figure 14 and Figure 15 presents sample data repeatabiltiy of the *uncorrected* forces and moments for both phases of the test in the form of delta force and moment coefficients, with respect to the average value for each angle of attack. The solid horizontal lines represent the 2σ limits based on the entire angle-of-attack range. Both comparisons shown are for active blowing through the circulation control slot, but analysis of the unpowered runs provided similar repeatability bands. The application of the new pressure tare correction will also impact the data accuracy analysis.

	Test	Run	Mach	Temp (deg F)	ReC (million)	NPR	Cmu
○	195	71	0.200	90.0	5.11	1.53	0.106
□	195	74	0.200	90.0	5.11	1.53	0.107
◇	195	77	0.200	90.3	5.11	1.53	0.106

Dotted lines indicate 95% balance accuracies obtained from calibration data. Solid lines indicate 2-sigma limits based on the data themselves.
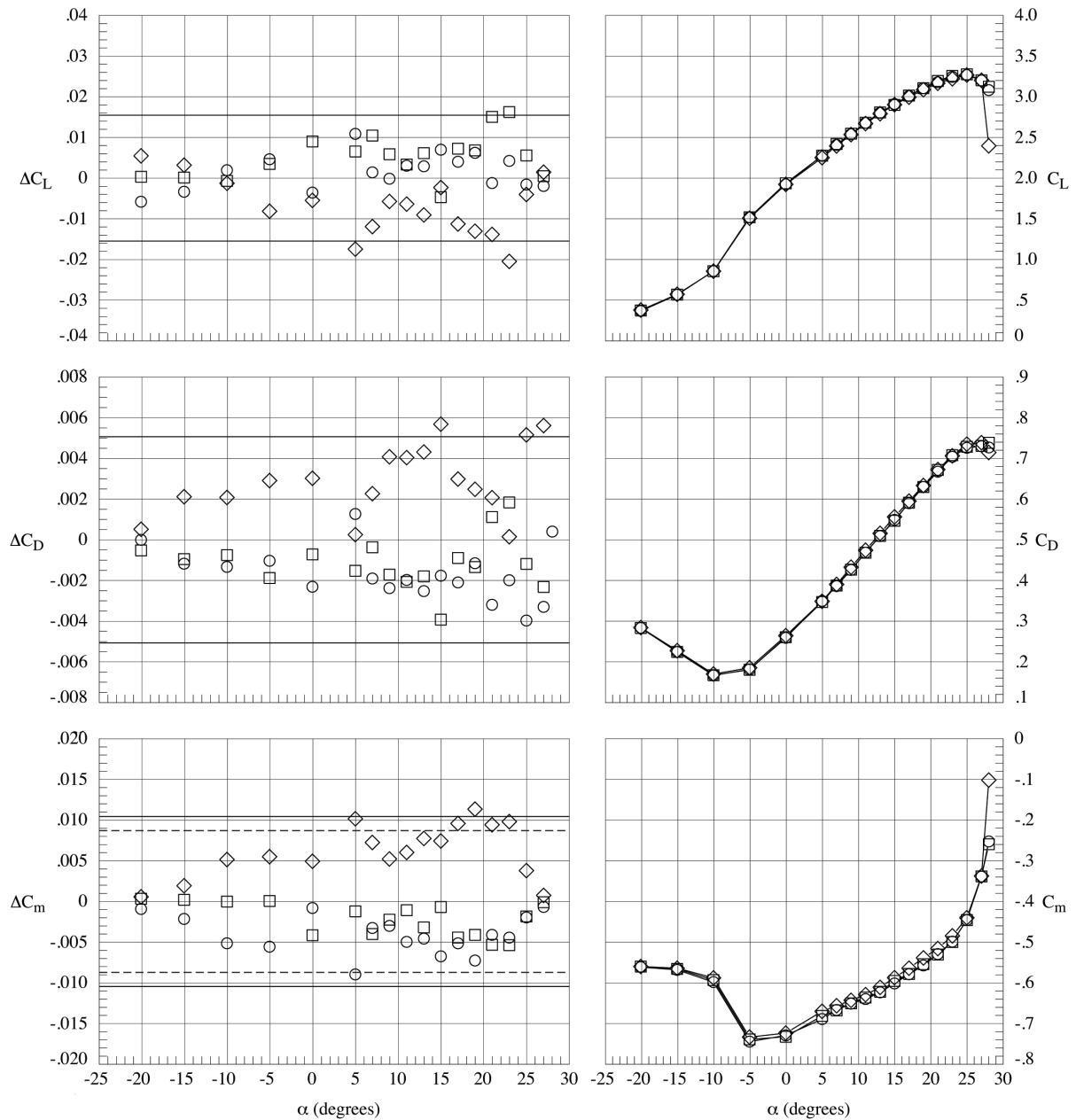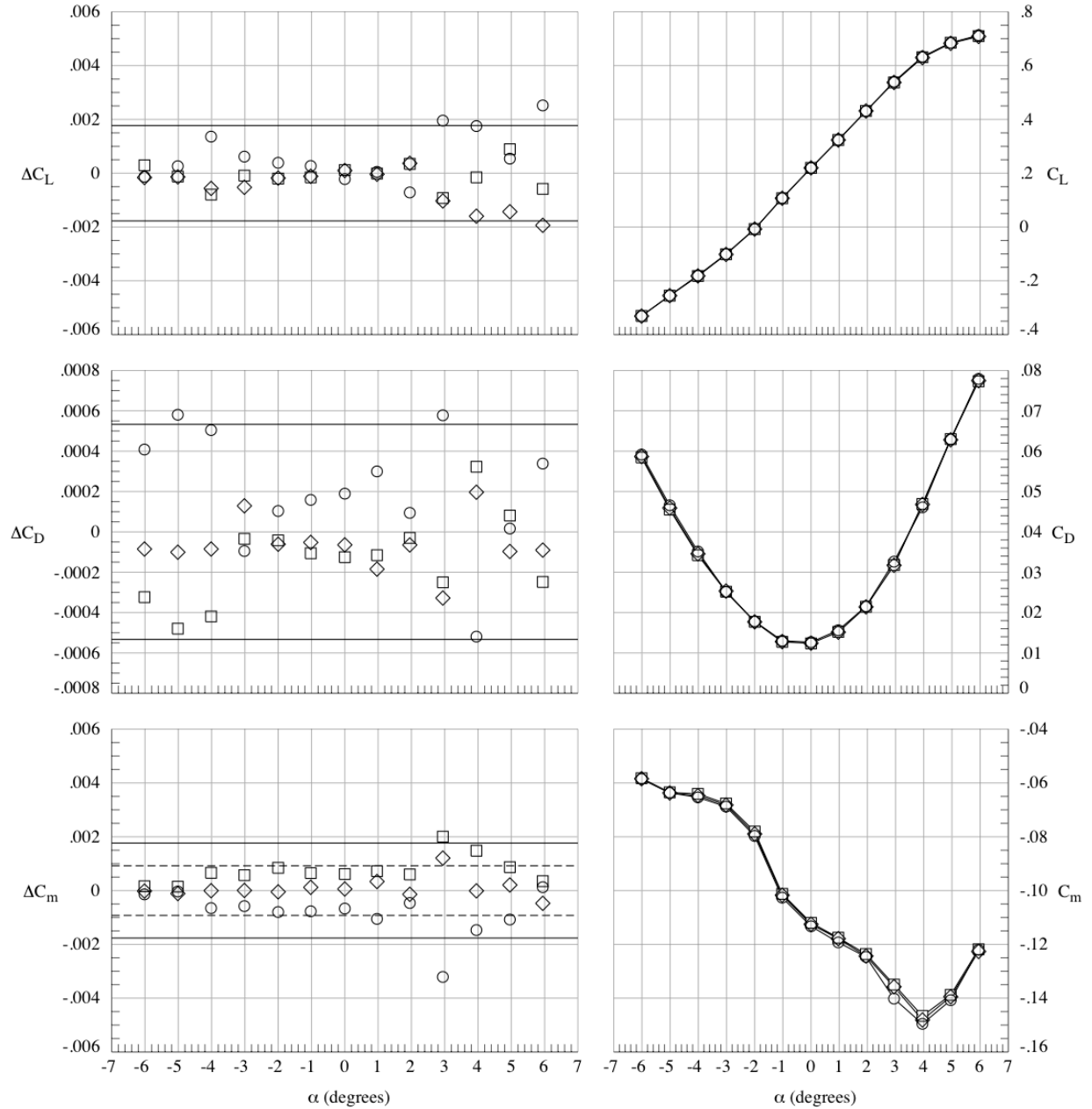

Figure 14: Repeatability of *uncorrected* force and moment data for the FAST-MAC model in the high-lift configuration (M_∞=0.20, Re=5x10^{6}). Solid horizontal lines represent the 2-sigma limits based on the residual data.

	Test	Run	Mach	Temp (deg F)	ReC (million)	NPR	Cmu
○	195	198	0.850	-50.3	20.02	1.55	0.004
□	195	206	0.849	-51.1	20.07	1.53	0.004
◇	195	207	0.850	-51.2	20.08	1.52	0.004

Dotted lines indicate 95% balance accuracies obtained from calibration data. Solid lines indicate 2-sigma limits based on the data themselves.

Figure 15: Repeatability of *uncorrected* force and moment data for the FAST-MAC model in the cruise configuration (M_∞=0.85, Re=20x10^6). Solid horizontal lines represent the 2-sigma limits based on the residual data.

American Institute of Aeronautics and Astronautics

B. Low-Speed High-Lift Testing

The high-lift performance of the FAST-MAC configuration is demonstrated by the NPR sweep at $\alpha = 0°$ shown in Figure 16, where the uncorrected lift coefficient data is presented for Mach numbers of 0.10 and 0.20. The effectiveness of the blowing over the dual radius flap is related to the wall bounded jet remaining attached to the flap throughout the blowing matrix. The first region, $C_\mu < 0.075$, is typically termed the separation control region, because the rapid increase in lift coefficient is due to the blowing progressively moving the flap separation to the trailing edge. At this point, the flap is fully attached, and the *uncorrected* lift coefficient has increased by 192%. The $M_\infty = 0.10$ data exhibits the classic super circulation behavior, where the lift continues to increase in a lower efficiency mode. In this regime, the wall bounded jet flow over the flap penetrates further into the oncoming flow field as illustrated by the example in Figure 3, further deflecting the streamlines and increasing the circulation. The $M_\infty = 0.20$ case however experiences an unexpected complete loss of lift enhancement when C_μ increases beyond 0.10.
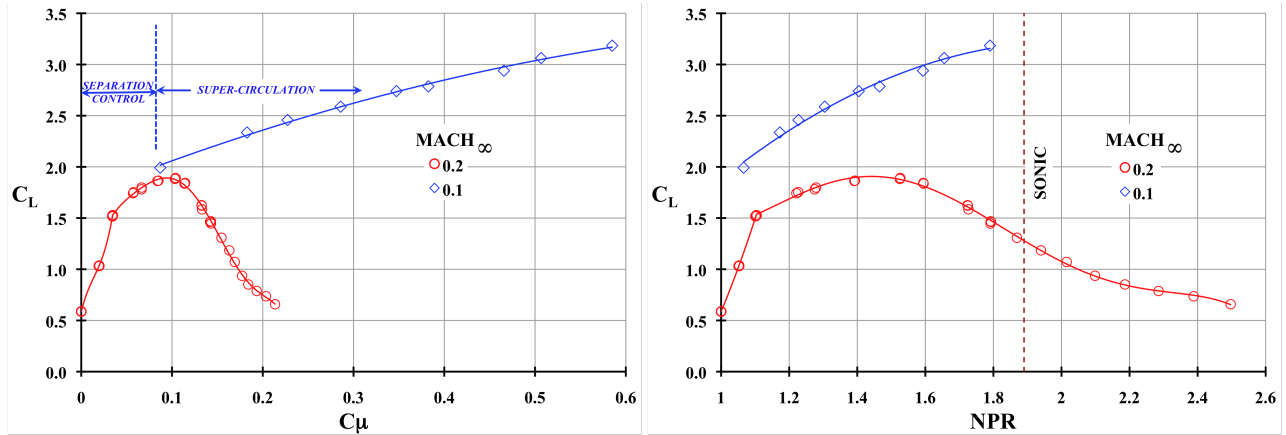

Figure 16: Effect of blowing on FAST-MAC high lift performance for 60° flap ($\alpha = 0°$, Re=5x10^{6}, $(T_o)_{jet}$ =0°F).

The inability of the model to sustain the super-circulation at $M_\infty = 0.20$ is related to the jet turning on the first radius of the dual radius flap. The upper surface flap pressures are plotted as a function of the local arc length s, along the flap in Figure 17. The slot exit is at $s/c = 0.0$, while negative values represent the taps inside the aft plenum region. The blowing cases depict the set NPR as well as a new value, NPR_{exit}, based on the local pressure measurement at the slot exit plane. In the separation control region, the blowing has attached the flow on the flap as expected, but the set NPR differs from the computed value NPR_{exit} by 20%. Note that each NPR definition yields different values of ideal C_μ for each plenum, which are tabulated and summed in the figures, and will be discussed below. At the transition to super circulation, the character of the pressure distribution changes. A supersonic expansion occurs downstream of the slot exit, as noted by the pressure coefficient exceeding the sonic value of C_p^*. The computed value of $NPR_{exit} = 2.32$ supports this observation, as it too has exceeded the sonic value of 1.92. At the two inboard stations, the wall-bounded jet has separated from the flap. The last comparison at NPR=1.79, where the super circulation has failed, shows a complete separation of the blowing

American Institute of Aeronautics and Astronautics

jet from the flap at *s*/c = 0.15 and significant loss of lift. As noted earlier in the paper, the choke plates in each plenum did not choke, and it is unclear what role this may have played in the observed flow physics. A new set of choke plates have recently been fabricated, and bench top flow testing and surveys will soon begin, to verify adequate choke plate performance before the next tunnel entry.
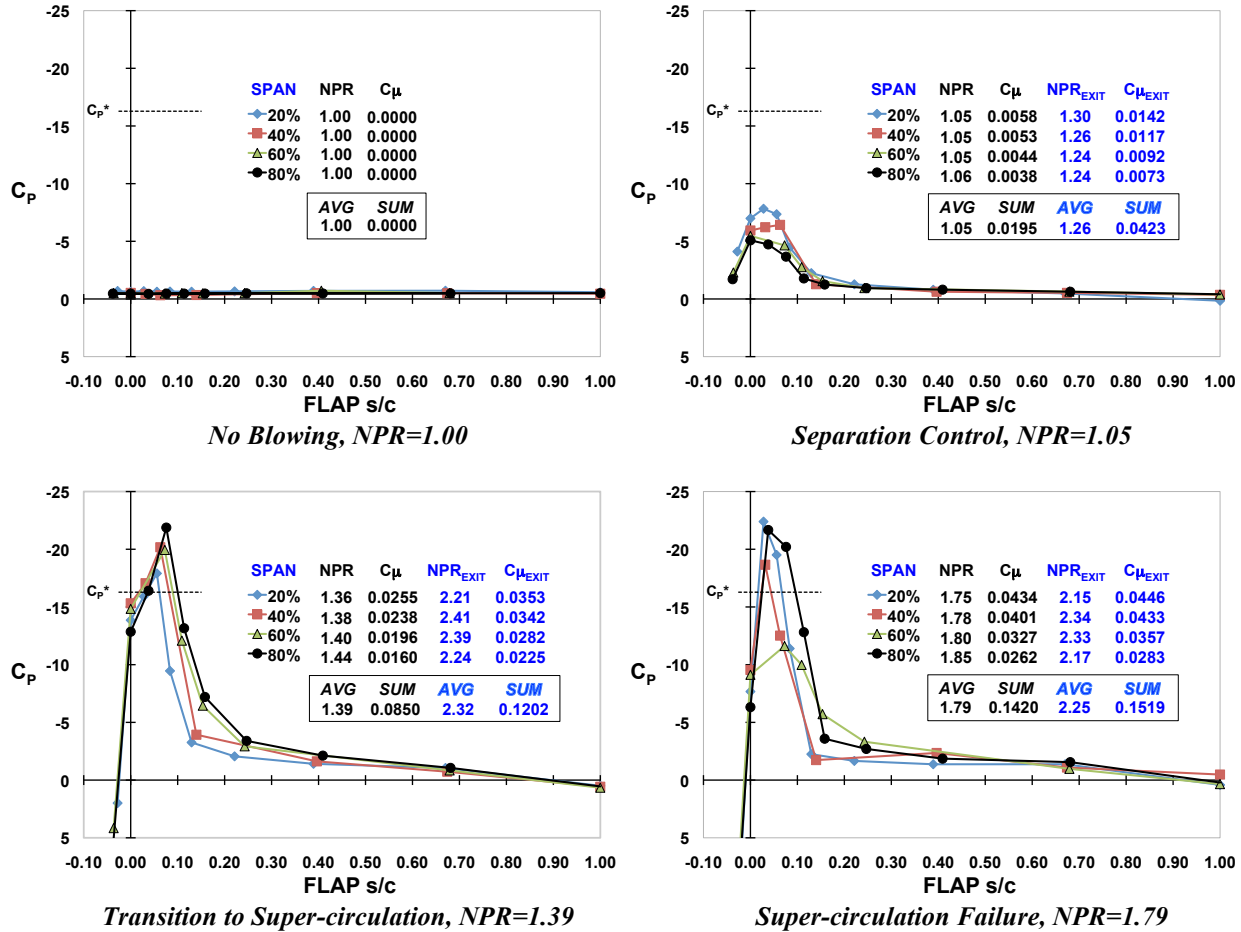

No Blowing, NPR=1.00

Separation Control, NPR=1.05

Transition to Super-circulation, NPR=1.39

Super-circulation Failure, NPR=1.79

Figure 17: **Comparison of spanwise flap pressures for three blowing conditions over the 60° flap (M_∞=0.20, α = 0.00°, Re=5x10^6, (T_o)$_{jet}$ =0°F).**

The recalculation of the ideal C_μ values for each plenum, based on the local slot exit static pressure, yields the comparison shown in Figure 18 for the same M_∞=0.20 data set. The original computed values of C_μ led to poor agreement with the measured mass flow from the air station MCV. The ideal mass flow values computed using local slot exit pressure show much better agreement with the
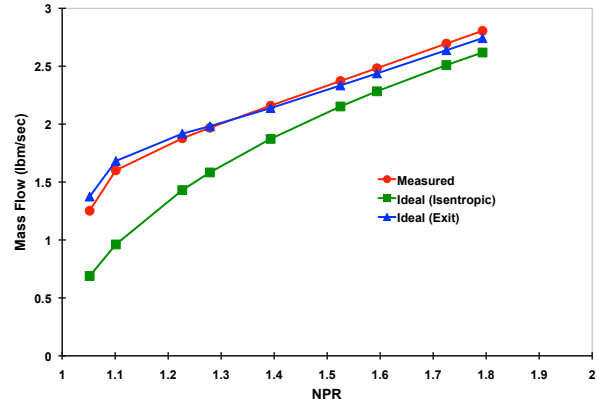

Figure 18: Comparison of ideal and measured mass flow using isentropic and jet exit conditions (M_∞=0.20, α = 0.0°, Re=5x10^6, (T_o)$_{jet}$ =0°F).

American Institute of Aeronautics and Astronautics

measured values, making it possible to compensate for the failure of the choke plates. This analysis will continue, but the remainder of the results presented in the paper will use the original definition of NPR.

Figure 19 examines the performance of the circulation control blowing across the angle-of-attack range where the *uncorrected* lift coefficient is plotted for two blowing cases at M_∞=0.20, and Re=15x10^6. Recall that NPR=1.20 is near the end of the separation control regime, whilst the NPR=1.50 case is in the super circulation control region, just before the wall bounded jet separates from the flap as discussed above. The blowing cases impart a near constant lift increment in the linear portion of the lift curve. Both blowing cases achieve maximum lift at α=25°, with the NPR=1.50 run increasing the maximum lift coefficient by approximately 33% as compared to the non-blowing case. Based on pre-test check loads applied to the model, it is anticipated that the bellows pressure tare correction will have minimal effect on this comparison.

run	NPR	
○	108.	1.00
□	113.	1.19
◇	109.	1.52
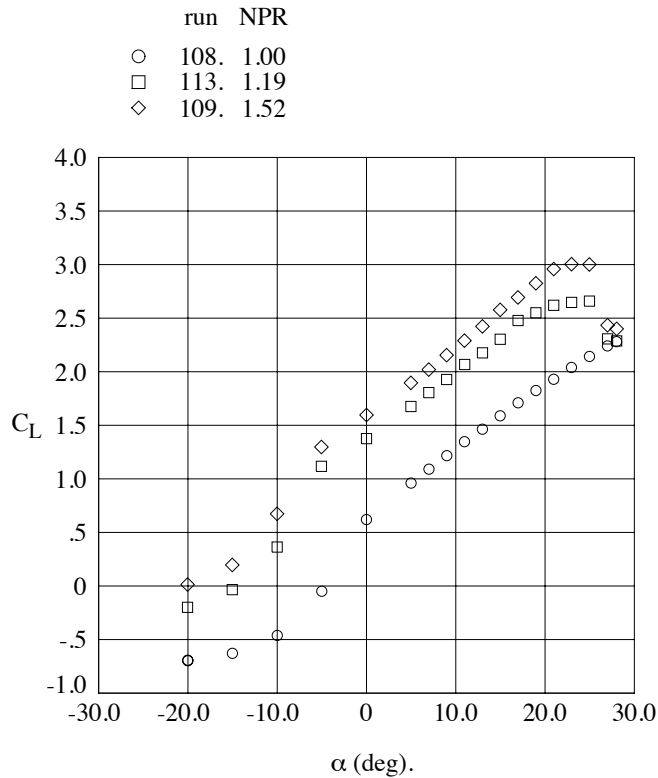
Figure 19: Effect of NPR on the *uncorrected* lift coefficient for the 60° flap
(M_∞=0.20,Re=15x10^6).

The impact of the blowing on the wing pressures is presented in Figure 20, for the same cases at α =23°. Note that each pressure plot includes a separate label key to indicate the local value of NPR for each plenum, where the plenums are numbered 1-4 moving inboard from the wing tip. Both blowing cases are in sharp contrast to the NPR=1.00 case, where the flap is completely separated. The NPR=1.50 condition shows a significant increase in the flap loading, which increases the lift as expected on all the three portions of the wing. Also of note is the small

14
American Institute of Aeronautics and Astronautics

sonic region on the outboard portion of the slat, which was one of the design objectives for the high-lift system[11]. The progression of the wing stall is explored in Figure 21, for NPR=1.50. As the angle-of-attack increases to 25°, the outboard flap is the first to exhibit flow separation just downstream of the slot exit. At 27° a complete loss of lift occurs at the outboard station, including the slat. The two inboard stations remain attached, but the $\eta = 0.60$ station may have experienced separation over the main wing portion. The next test entry of the FAST-MAC model will collect flow visualization data to more fully document the stall development.
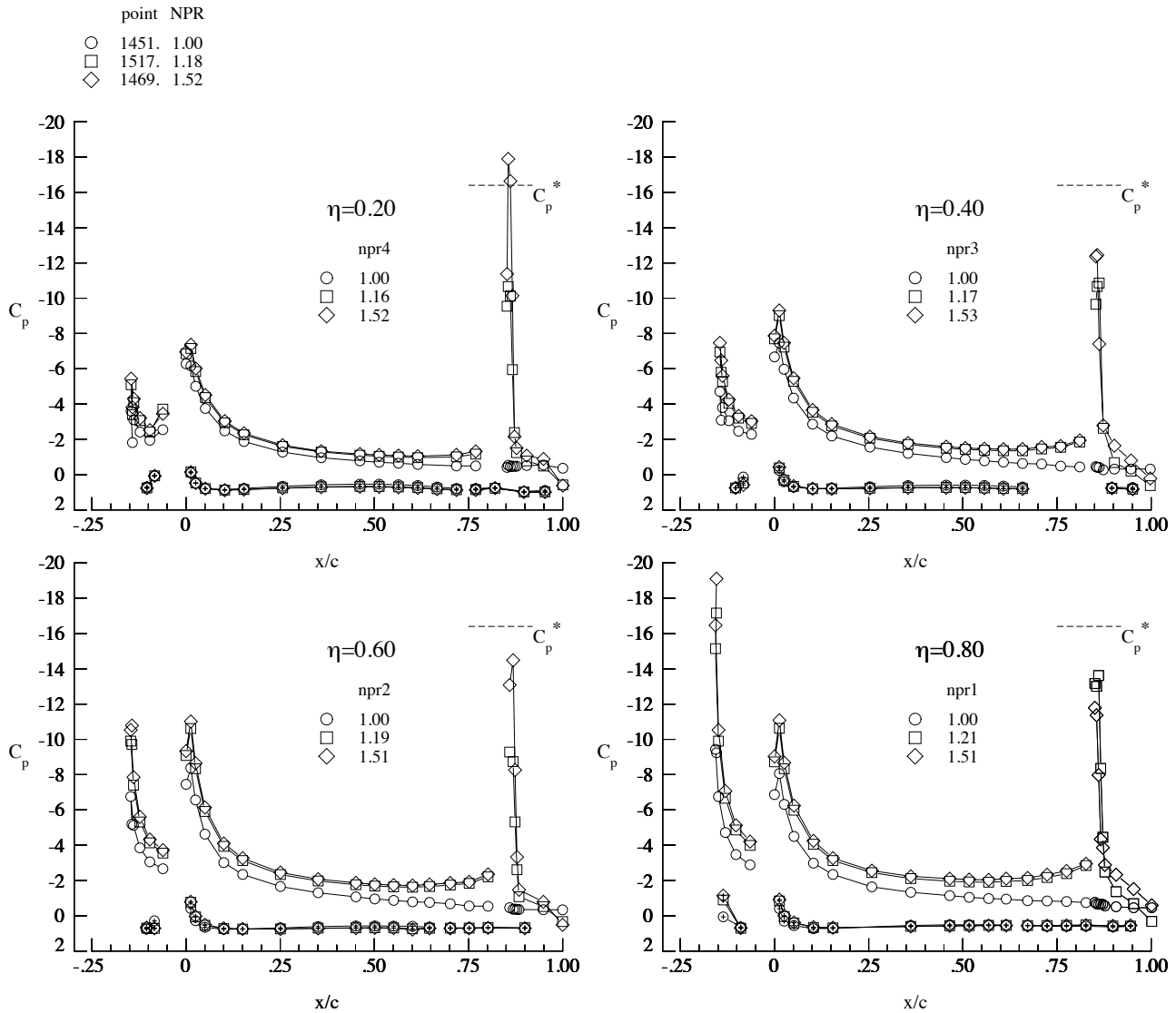
Figure 20: Effect of NPR on wing pressures near maximum lift for the 60° flap (M_∞=0.20, $\alpha = 23.00°$, Re=15x10^{6}).
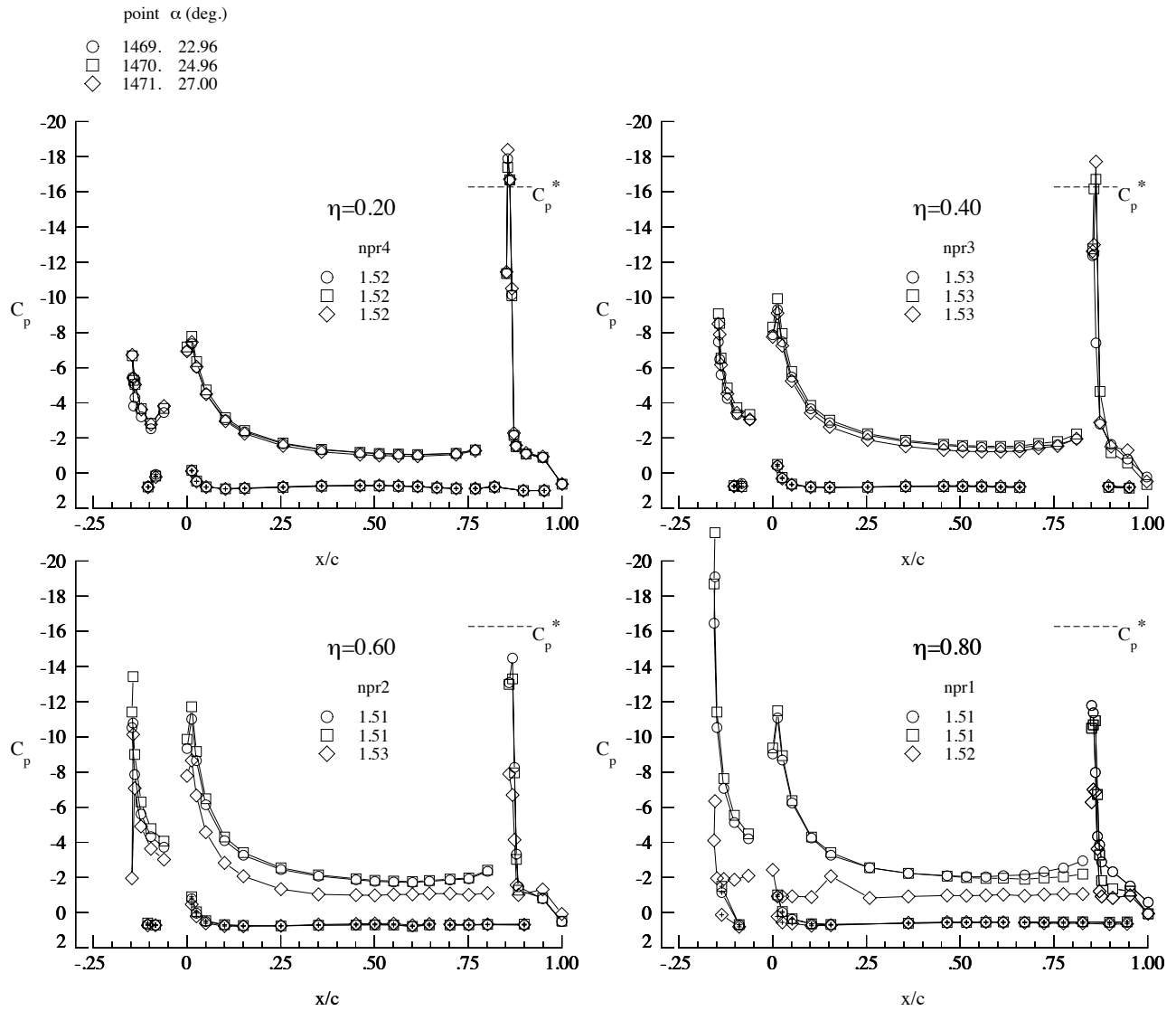
Figure 21: Progression of wing stall for the 60° flap (M$_\infty$=0.20, Re=15x10^6,NPR=1.50).

American Institute of Aeronautics and Astronautics

C. Transonic Cruise Testing

To examine the effect of blowing at transonic conditions, numerous NPR sweeps were performed at fixed angles-of-attack, at various combinations of Mach and Reynolds numbers. Figure 22 examines the effect of a low blowing rate on the wing pressures for $M_\infty=0.85$, $\alpha=3.00°$, and $Re=10\times10^6$. The non-blowing case, NPR=1.00, is close to the design point of the wing, and as such represents a well performing wing design with attached flow. The addition of the comparatively low velocity flow exiting the blowing slot has decelerated the flow over the cruise flap and caused the shockwave to move forward, creating a loss in lift across the entire wing. As the blowing is increased to NPR = 1.41 in Figure 23, the shockwave returns to the original location while an increase in lift occurs downstream of the blowing slot. Further increase of the blowing to NPR = 2.25 alters the shockwave structure, with the shock strength unchanged. The loading on the cruise flap has increased, and a lift increment now occurs on the lower surface of the entire wing. These comparisons have shown that the blowing slot can impact the wing aerodynamics for attached flow conditions by increasing the loading on the cruise flap. Further studies will be conducted using CFD and wind tunnel testing to investigate the ability of variable spanwise blowing to actively tailor the spanload distribution of the wing.
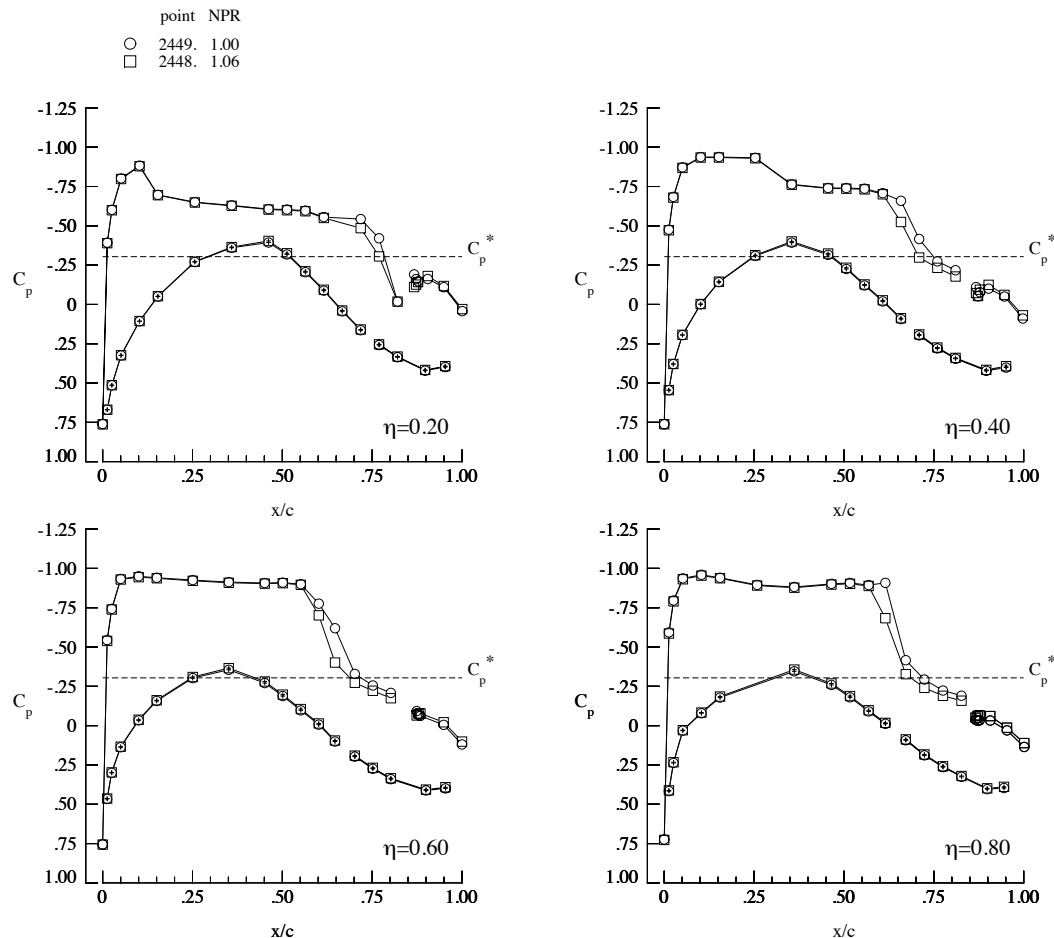

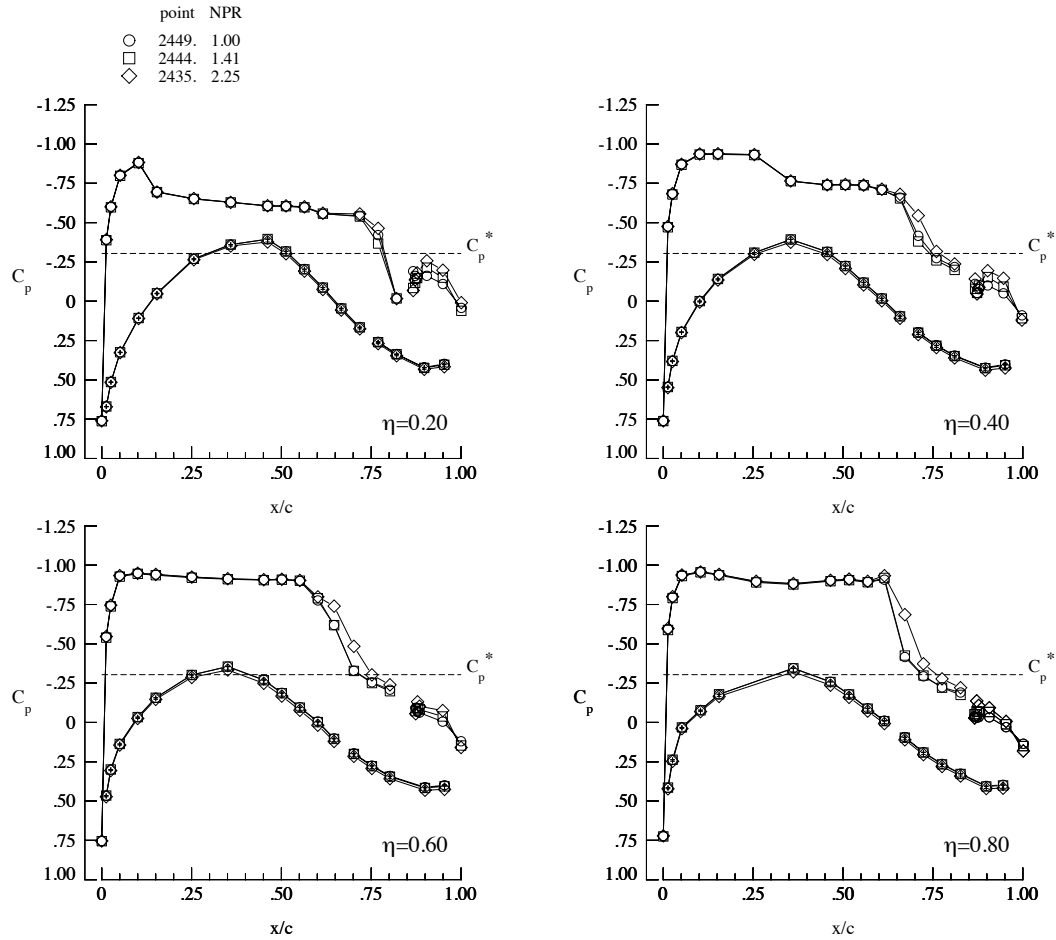Figure 22: Effect of low NPR on wing pressures ($M_\infty=0.85$, $\alpha = 3.00°$ $Re=10\times10^6$).

17

American Institute of Aeronautics and Astronautics

Figure 23: Effect of elevated NPR on wing pressures (M_∞=0.85, α = 3.00°, Re=10x10^6).

The use of the blowing slot at off-design conditions is explored in Figure 24, for M_∞=0.85, α = 3.92° and Re = 30x10^6. The wing pressures indicate flow separation on the outboard portion of the wing for the non-blowing case, NPR=1.0. The addition of blowing, NPR=1.53, reattaches the boundary layer and moves the shockwave aft by 5% chord. The final case, NPR=2.48, has moved the shockwave aft for the three outboard stations by another 5% chord. It is significant to note that the shockwave strength did *not* increase for this increase in blowing, and it can be inferred that the wave drag has not increased. To quantify the effect on the drag coefficient, the bellows pressure tare must be applied, and the added thrust properly accounted for. Similar results were obtained at Mach numbers of 0.86 and 0.87.
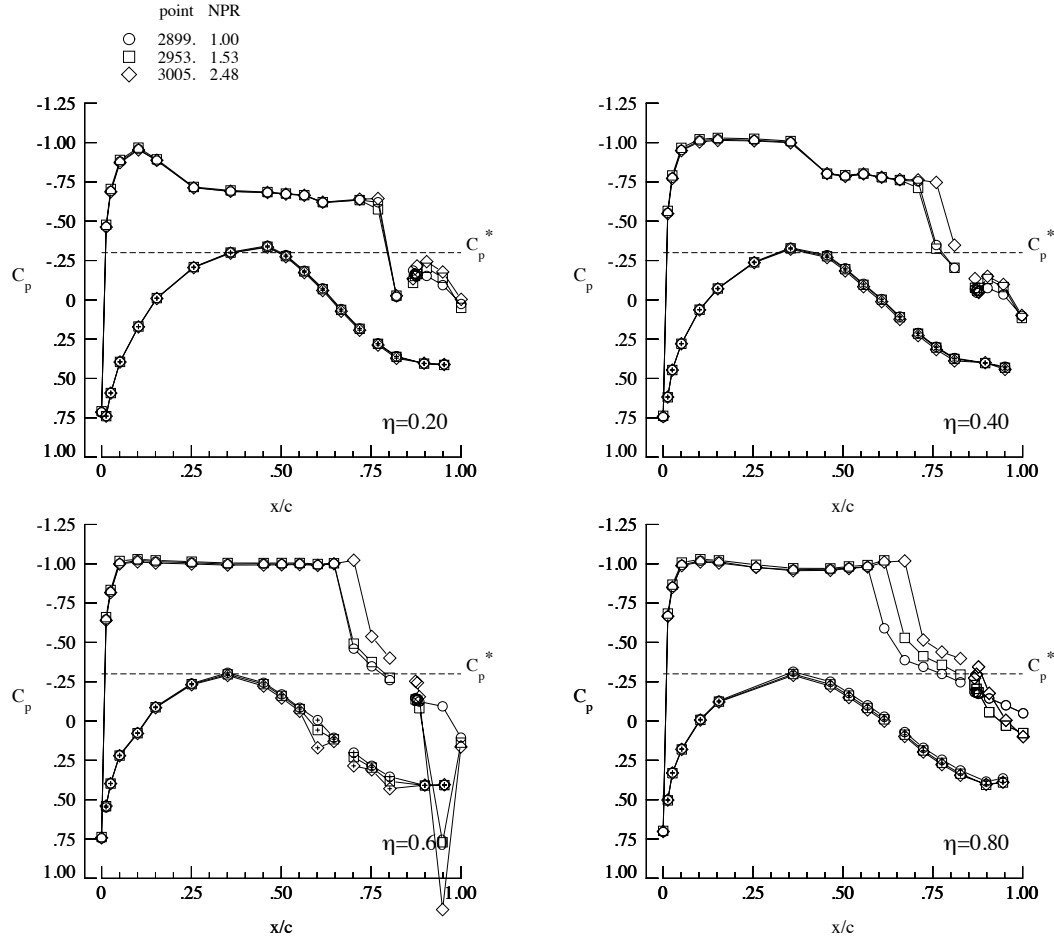
American Institute of Aeronautics and Astronautics

Figure 24: Effect of NPR on wing pressures at off-design conditions (M_∞=0.85, α = 3.92°, Re=30x10^6).

Studies were also conducted to explore the effect of only blowing near the tip of the wing, to reduce the required mass flow. Figure 25 presents the wing pressure comparison for M_∞=0.85, α = 3.92° and Re = 15x10^6. As above, the outboard row indicates the presence of flow separation in the trailing edge region. Blowing from the two outboard plenums, at a nominal NPR of 2.6, again attached the flow and shifted the shockwave aft at both stations. The final case of blowing only through the outboard plenum, NPR1 = 2.45, did attach the flow and alter the shockwave pattern. The blowing effect did carry over to slightly increase the cruise flap loading at η = 0.60. Although not presented, NPR sweeps were conducted for blowing only through plenum-1, to further document its flow control authority. Of particular note were the observed changes to the rolling moment coefficient, suggesting that pneumatic based roll control would be possible.
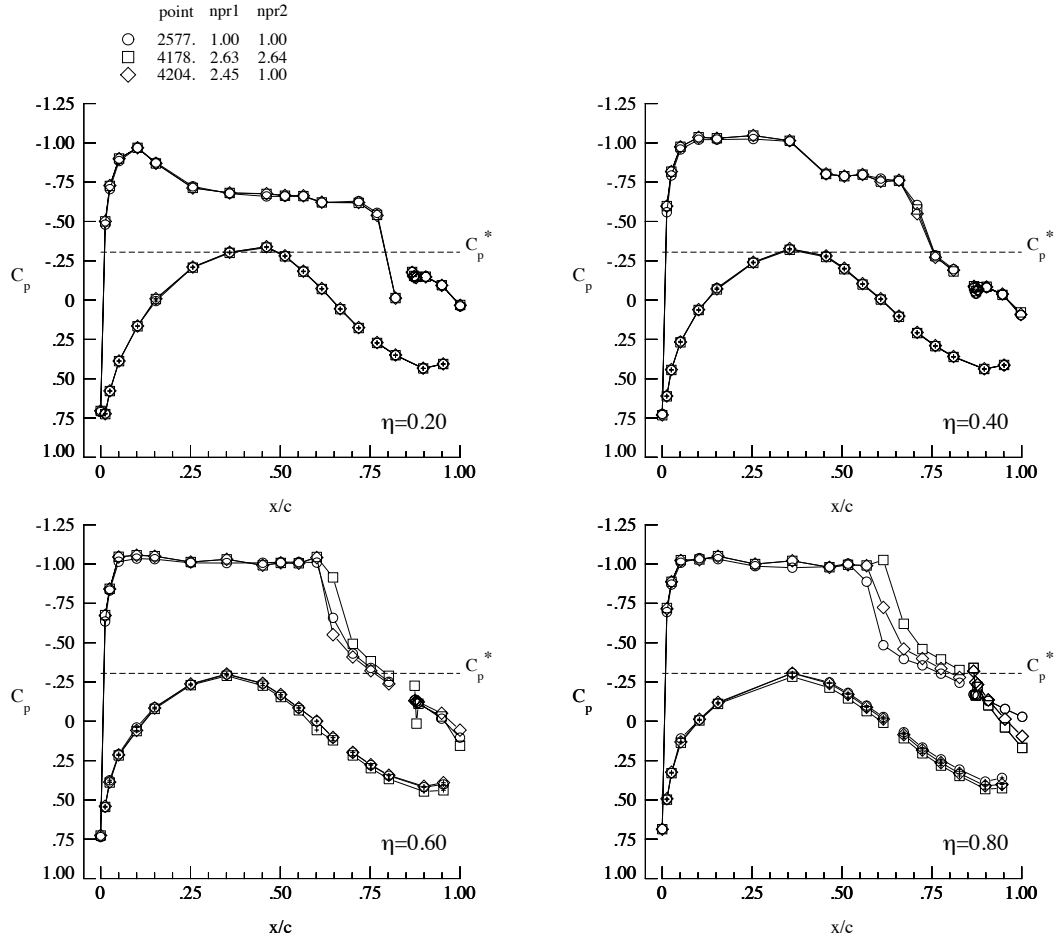
American Institute of Aeronautics and Astronautics

Figure 25: Effect of outboard blowing on wing pressures at off-design conditions (M_∞=0.85, α = 3.92°, Re=15x10^6).

IV. Conclusions

The FAST-MAC model testing in the National Transonic Facility represents the first active flow control test performed at the facility, as well as the first transonic semi-span test, and the first use of the new NTF-117S semi-span force and moment balance. The model was configured to test circulation control strategies at realistic flight Reynolds numbers over a wide range of freestream Mach numbers. The model was equipped with four onboard flow control valves, which allowed for independent control of the circulation control flow paths, which were directed over a 15% chord simple-hinged flap. The preliminary analysis of the *uncorrected* lift data was corroborated by the wing pressure data, which also provided key insight into the complex flow physics of the circulation control blowing.

For the low-speed high-lift testing, the circulation control was directed over a 60° simple-hinged trailing edge flap, while a conventional slat was mounted on the leading edge. Testing was primarily conducted at a Mach number of 0.20, but a limited dataset was obtained at a Mach number of 0.10. The chord Reynolds number was varied from 5×10^6 to 15×10^6. At zero degrees angle-of-attack, the circulation control nearly doubled the lift coefficient of the model in the separation control regime. At a Mach number of 0.20, the model was not able to completely support the development of super circulation. The premature wall bounded jet separation on the flap may be attributed to possible non-uniformity in the individual flow paths caused by the poor performance of the aft plenum choke plates. It is also possible that the slot height was too large resulting in a high momentum condition that combined with the supersonic expansion over the first radius of the flap could have caused the premature wall bounded jet separation on the flap. The circulation control blowing was still shown to provide a near constant lift increment over the linear portion of the lift curve, and increased the *uncorrected* maximum lift coefficient by 33% at the highest Reynolds number. The stall pattern of the wing was observed to begin with flow separation on the outboard portion of the actively blown flap.

The transonic cruise testing was performed with a zero degree trailing edge deflection, at freestream Mach numbers ranging from 0.70 to 0.88, while the chord Reynolds number was varied from 10×10^6 to 30×10^6. The addition of low blowing rates at the Mach 0.85 design condition of the wing resulted in a loss of lift and forward movement of the shockwave. Increasing the blowing rate restored the lift and returned the shockwave to the original location and strength, while increasing the loading over the cruise flap. Application of the circulation control to off-design conditions demonstrated the ability to reattach separated flow on the cruise flap, and shift the shockwave aft, while maintaining the original shock strength. Lastly, blowing only over the outboard portion of the cruise flap was beneficial, and demonstrated the feasibility of a pneumatic based roll control capability.

Considerable progress has been made in developing testing methods for active flow control techniques and propulsion simulations at the National Transonic Facility. To further quantify the benefits of the circulation control technique at flight Reynolds numbers, the new pressure tare correction for the bellows will be applied to the wind tunnel data. A thrust removal strategy must also be developed to account for the added thrust components. Improved choke plates are being fabricated for the FAST-MAC model and will be bench tested before the next tunnel entry in 2012. Lastly, new CFD studies are underway to more accurately model the as-built model geometry, and complement the analysis of the experimental dataset that has been generated.

Acknowledgements

References

[1] Zeune, C.H., "Enabling Speed Agility for the Air Force", AIAA Paper 2010-349, January 2010.

[2] Collins, S. W., Westra, B. W., Lin, J. C., Jones, G. S., and Zeune, C. H., "Wind Tunnel Testing of Powered Lift, All-Wing STOL Model," RAeS–566–5A3, presented at the 2008 International Powered Lift Conference, London, UK, July 2008.

[3] Jones, G.S., Joslin, R.D., "Proceedings of the 2004 NASA/ONR Circulation Control Workshop", NASA/CP-2005-213509, June 2005.

[4] Englar, R. J., "Development of the A-6 Circulation Control Wing Flight Demonstrator Configuration," DTNSRDC Report ASED-79/01, January, 1979.

[5] Rogers, E.O., Donnelly, M.J., "Characteristics of a Dual-Slotted Circulation Control Wing of Low Aspect Ratio Intended for Naval Hydrodynamic Applications," AIAA Paper 2004-1244, January 2004.

[6] Jones, G.S, Lin., J.C., Allan, B.G., Milholen II, W.E., Rumsey, C.L., and Swanson, R.C., "Overview of CFD Validation Experiments for Circulation Control Applications at NASA", International Powered Lift Conference, Royal Aeronautical Society, London, July 2008.

[7] Englar, R.J., G.S. Jones, B.G. Allan, and J.C. Lin, "2-D Circulation Control Airfoil Benchmark Experiments Intended for CFD Code Validation," AIAA Paper 2009-0902, January 2009.

[8] Swanson, R.C. and Rumsey, C.L., "Numerical Issues for Circulation Control Calculations," AIAA Paper 2006-3008, June 2006.

[9] Pfingsten, K.C and Radespiel, R., "Experimental and Numerical Investigation of a Circulation Control Airfoil", AIAA Paper 2009-533, January 2009.

[10] Wetzel, D., Griffin, J., Liu, F., and Cattafesta, L., "An Experimental Study of Circulation Control on an Elliptic Airfoil", AIAA Paper 2009-4280, June, 2009.

[11] Milholen II, W.E., Jones, G.S., and Cagle, C.M., "NASA High-Reynolds Number Circulation Control Research - Overview of CFD and Planned Experiments (Invited)", AIAA Paper 2010-344, January 2010

[12] Englar, R. J., Smith, M. J., Kelley, S. M., and Rover, R. C. III, "Application of Circulation Control Technology to Advanced Subsonic Transport Aircraft, Part I: Airfoil Development," AIAA Paper No. 93- 0644, AIAA *Journal of Aircraft*, Vol. 31, No. 5, pp. 1160-1168, Sept-Oct. 1994.

[13] Englar, R.J., "Two- Dimensional Transonic Wind Tunnel Tests of Three 15-Percent –Thick Circulation Control Airfoils," Naval Ship R&D Center Technical Note AL-182, AD 882-075, December 1970.

[14] Jones, G.S., Yao, C., Allan, B.G., "Experimental Investigation of a 2D Supercritical Circulation-Control Airfoil Using Particle Image Velocimetry," AIAA 2006-3009, June 2006.

[15] Anderson, S.B., Quigley, H.C., and Innis, R.C., "Flight Measurements of the Low-Speed Characteristics of a 35° Swept-Wing Airplane with Blowing-Type Boundary-Layer Control on the Trailing-Edge Flaps", NACA RM-A56G30, October 1956.

[16] Englar, R.J., Williams, R.M., "Test Techniques for High Lift, Two-Dimensional Airfoils with Boundary Layer and Circulation Control for Applications to Rotary Wing Aircraft", Canadian Aeronautics and Space Journal, Vol.19, No.3, March 1973.

[17] Jones, G.S., Milholen II, W.E., and Goodliff, S.L., "Development of the Dual Aerodynamic Nozzle Model for the NTF Semi-Span Model Support System", AIAA Paper 2011-3170, June 2011.

[18] Gatlin, G.M, Tomek, W.G., Payne, F.M., and Griffiths, R.C., "Recent Improvements in Semi-Span Testing at the National Transonic Facility (Invited)", AIAA Paper 2006-508, January 2006.

[19] Manning, B., Doussin, J.F., "Best Practices in the use of "Smart" Displacement, Gap and Hole Mapping Sensors for Aircraft and Aircraft Engine test and overhaul", Aerospace Texting Expo 2005, Hamburg, Germany, *April 6, 2005.*

[20] Lynn, K.C., "Development of the NTF-117S Semi-Span Balance", AIAA Paper 2010-4542, June 2010.

[21] Berrier, B.L., Leavitt, L.D., and Bangert, L.S., "Operating Characteristics of a Multiple Critical Venturi System and Secondary Calibration Nozzles Used for Weight-Flow Measurements in the Langley 16-Foot Transonic Tunnel", NASA TM-96405, September 1985